# Concurrent Dual Polarization Dielectric Waveguide Interconnect using Inverse Designed Dual-Mode Surface Antenna Launcher

Jui-Yu Huang, Andreas F. Molisch, and Constantine Sideris

Department of Electrical and Computer Engineering, University of Southern California, Los Angeles, CA 90089, USA

Abstract—We present the design of a dual-mode metallic antenna coupler that can simultaneously couple two separate signals into orthogonal polarizations of a dual-polarization metalcoated dielectric waveguide. The coupler sits on the top surface of the waveguide and features two side-by-side excitation ports, which excite the  $E_x$  polarization of the waveguide when driven differentially and the  $E_y$  polarization when driven in common mode. Design is done using random coordinate ascent (RCA). Simulation results show that both modes can be operated simultaneously in the 88.6-94 GHz range, achieving 6% fractional bandwidth and a coupler-to-coupler channel insertion loss of 3dB per channel. Due to the symmetric design of the coupler, the interconnect has theoretically zero cross-coupling between the two polarization channels. The design is also amenable to fabrication via standard microfabrication techniques due to its single-plane surface coupling nature. To the best of our knowledge, this is the first realization of a concurrent dual-mode dielectric waveguide which leverages a single surface antenna for coupling into both modes simultaneously.

### I. Introduction

Waveguide links have drawn increasing attention in recent years as they can offer better efficiency at high carrier frequencies and bandwidths than traditional copper wireline. A number of techniques have been investigated for efficiently coupling energy into and out from dielectric waveguides, including vertical end-launchers such as [1], [2], which use a parasitic patch to couple energy from the end-faces into the TE10 mode, as well as surface launchers, such as [3], [4], which use a folded slot transition and through-patch coupling respectively. Due to their vertical orientation, vertical end-launchers can be challenging to fabricate using planar lithographic techniques, especially in the case of metalcoated waveguides. Surface-based launchers, on the other hand, are compatible with standard microfabrication techniques; however, surface launchers that can couple simultaneously into both modes of metal-coated dielectric waveguides which support two orthogonal polarizations have not yet been explored. Utilizing multiple modes, also known as modedivision multiplexing, can increase the data rate available in a communication link or facilitate full-duplex communication by using a different mode for each direction. In this paper, we present a dual-mode metallic surface coupling antenna, inverse designed using a random coordinate ascent (RCA) tile-flipping algorithm, which can be patterned onto the top surface of a square cross-section shielded dielectric waveguide and can efficiently and can achieve dual channel operation by simultaneously coupling into both orthogonal polarizations.

# II. OPTIMIZATION ALGORITHM

The surface coupler is parametrized by using a uniform 21×21 Cartesian grid composed of square tiles, each of which can be filled with metal or left open exposing the dielectric surface as shown in Fig. 1. Mirror symmetry is enforced during the optimization of the coupler design with respect to the longitudinal plane due to the symmetry exhibited by the two lowest cut-off modes of the square waveguide. The antenna is driven by two side by side ports at the bottom edge. Specifically, common-mode and differential-mode excitation of these two ports is used to excite the vertically polarized and horizontally polarized E-field modes, respectively. Since the tiles corresponding to the driving ports and the ones adjacent to them are not allowed to change, 223 total tiles can be optimized, resulting in a formidable optimization problem supporting  $2^{223}$  possible solutions. To find a design with favorable performance, we adopted RCA [5] as the optimization strategy and used the commercial 3D FDTD solver, CST, to evaluate candidate designs. To enhance the bandwidth of operation, a non-linear multi-objective function is used to concurrently optimize the coupling efficiency into each polarization while minimizing the return loss [6]. The following objective was maximized:

$$F = \sum_{n=1}^{N} \left[ \prod_{m \neq n}^{N} logsig(a + b \cdot x_m) \right] \cdot x_n, \tag{1}$$

where

$$x_n = \sum_{q=1}^{3} \left[ \prod_{p \neq q}^{3} logsig(c_p + d_p \cdot y_{n,p}) \right] \cdot y_{n,q}$$
 (2)

$$y_{n,1} = (1 - |S_{cc11}(f_n)|^2)^2 + (|S_{cc21}|^2)^2,$$
 (3)

$$y_{n,2} = (1 - |S_{dd11}(f_n)|^2)^2 + (|S_{dd21}|^2)^2,$$
 (4)

$$y_{n,3} = (1 - |S_{dc11}|^2)^2, (5)$$

 $(a,b)=(-2.24,1.39),\ (c_1,d_1)=(-3.82,4.37),\ (c_2,d_2)=(c_1,d_1),\ (c_3,d_3)=(-4.69,6.89),\ \ {\rm and}\ \ logsig(x)=\frac{1}{1+\exp(-x)}.$  The design is optimized at N=8 frequencies to achieve broadband performance, sampling the mixed-mode S-parameters between 82.5 and 100GHz at 2.5GHz intervals. Coefficients (a,b) and (c,d) are used to adjust the logsig function's limiting behavior.  $x_n$  represents the objective function for each individual frequency, and the product of logsig(x) terms with each  $x_n$  represent nonlinear weights

which place emphasis on underperforming frequencies—the  $logsig(a+b\cdot x_m)$  function behaves like a switch: as  $x_m$  exceeds an upper performance threshold,  $logsig(a+b\cdot x_m)$  saturates, reducing the emphasis of that  $x_m$  term and increasing the importance of the other frequencies. Each  $x_n$  in (2) is comprised of three sub-objectives  $(y_{n,q})$ : maximize common-mode to common-mode transmission  $(S_{cc21})$ , maximize differential-mode to differential-mode transmission  $(S_{dd21})$ , and minimize local differential to common-mode cross-coupling  $(S_{dc11})$ . The coefficients,  $c_1, d_1, c_2, d_2$  were chosen such that the logsig activation functions saturate for  $S_{cc11}$  and  $S_{dd11}$  better than -10dB and for  $S_{cc21}$  and  $S_{dd21}$  better than -2dB.  $c_3$  and  $d_3$  are chosen such that the logsig function corresponding to the cross-coupling saturates for  $S_{dc11}$  better than -30dB.

# III. SIMULATION RESULTS

A waveguide with polyimide ( $\epsilon_r = 3.5$  and  $\tan \delta = 0.008$ ) core and 1mm×1mm size cross-section was used, correspond ing to a usable frequency range from 80 to 113GHz for dua mode propagation. The simulated length of the waveguide 6mm. Fig. 1 shows the end-to-end link with both surfac couplers, and the inset shows a top-down view of the fin: optimized coupler. Fig. 2 shows the E-field profiles produce by common-mode and differential-mode excitations in th cross-section of the waveguide. Fig. 3 plots the objective function vs. iteration and the insertion and return losses for each mode. Due to mirror symmetry, the theoretical crosscoupling  $(S_{dc11})$  is 0. The simulated  $|S_{cc11}|$  and  $|S_{dd11}|$ return losses are both below -10 dB from 88.6 to 94 GHz, corresponding to a 6% fractional bandwidth (FBW). It may be possible to further improve the bandwidth by increasing the number of frequencies used in the optimization.

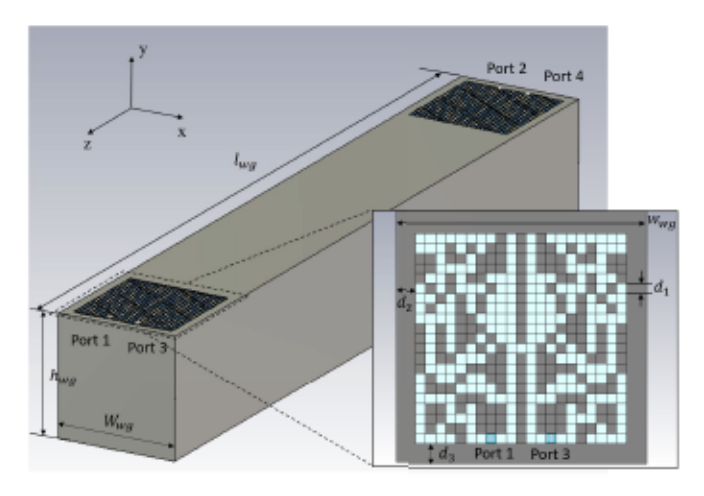


Fig. 1. Perspective view of entire system. Dimensions:  $w_{wg}=1 \mathrm{mm}$ ,  $h_{wg}=1 \mathrm{mm}$ , and  $l_{wg}=6 \mathrm{mm}$ . Ports 1 and 3 form a differential pair for one coupler, and ports 2 and 4 are on the other coupler. Optimized antenna:  $d_1=40 \mu \mathrm{m}$ ,  $d_2=80 \mu \mathrm{m}$ , and  $d_3=80 \mu \mathrm{m}$ 

## IV. CONCLUSION

We have explored the potential of using RCA and have designed, for the first time, a planar transition to a metallic-

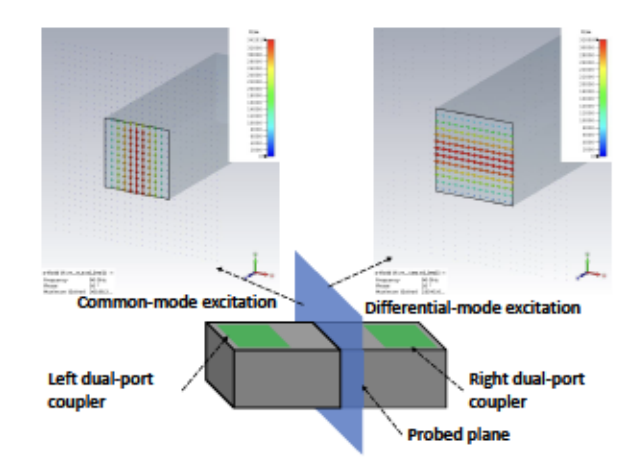


Fig. 2. Simulated E-field vector plots of waveguide cross-section for common-mode and differential-mode excitations.

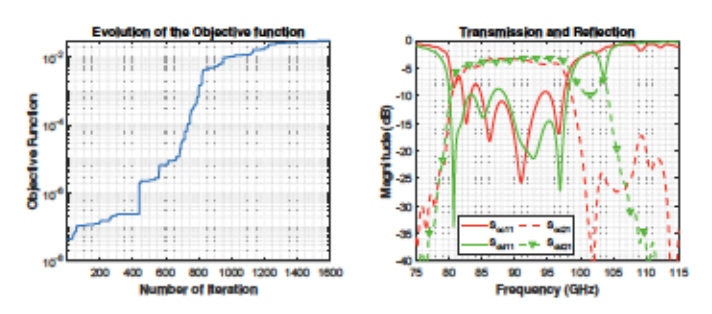


Fig. 3. Objective function vs. number of iteration and simulated S-parameters of link.

coated dielectric waveguide that can couple into two polarizations concurrently using a single antenna. The design is also compatible for on-chip or on-printed circuit board integration due to its planar nature.

# REFERENCES

- N. Thanh Tuan, K. Sakakibara and N. Kikuma, "Bandwidth Extension of Planar Microstrip-to-Waveguide Transition by Controlling Transmission Modes Through Via-Hole Positioning in Millimeter-Wave Band," in *IEEE Access*, vol. 7, pp. 161385–161393, 2019, doi: 10.1109/AC-CESS.2019.2952073.
- [2] G. C. Dogiamis et al., "A 60-Gbps 108-GHz 16-QAM Dielectric Waveguide Interconnect with Package Integrated Filters," 2022 IEEE/MTT-S International Microwave Symposium - IMS 2022, Denver, CO, USA, 2022, pp. 556–559, doi: 10.1109/IMS37962.2022.9865352.
- [3] G. Gentile et al., "Silicon-Filled Rectangular Waveguides and Frequency Scanning Antennas for mm-Wave Integrated Systems," in *IEEE Trans*actions on Antennas and Propagation, vol. 61, no. 12, pp. 5893–5901, Dec. 2013, doi: 10.1109/TAP.2013.2281518.
- [4] J. Sorocki et al., "Additively Fabricated Air-Filled Waveguide Integrated With Printed Circuit Board Using a Through-Patch Transition," in *IEEE Microwave and Wireless Components Letters*, vol. 31, no. 11, pp. 1207–1210, Nov. 2021, doi: 10.1109/LMWC.2021.3112567.
- [5] C. Sideris et al., "Automated design of a 3D printed waveguide surface coupler," in 2015 IEEE International Symposium on Antennas and Propagation & USNC/URSI National Radio Science Meeting, Vancouver, BC, Canada, 2015, pp. 318–319, doi: 10.1109/APS.2015.7304545.
- [6] M. R. Khan, C. L. Zekios, S. Bhardwaj and S. V. Georgakopoulos, "Multiobjective Fitness Functions With Nonlinear Switching for Antenna Optimizations," in *IEEE Open Journal of Antennas and Propagation*, vol. 3, pp. 613–626, 2022, doi: 10.1109/OJAP.2022.3178840.